International Journal of Refractory Metals and Hard Materials 111 (2023) 106079

Contents lists available at ScienceDirect

International Journal of Refractory Metals and Hard Materials

journal homepage: www.elsevier.com/locate/IJRMHM

The effect of microstructure evolution on the wear behavior of tantalum processed by Indirect Extrusion Angular Pressing

Babak Omranpour Shahreza [a,b,c,*], Jacques Huot [b], Maksim Antonov [a], Lembit Kommel [a], Fjodor Sergejev [a], Francisco Javier Pérez Trujillo [c], Anita Heczel [d,e], Jenő Gubicza [d]

[a] Department of Mechanical and Industrial Engineering, Tallinn University of Technology (TalTech), Ehitajate tee 5, Tallinn 19086, Estonia
[b] Hydrogen Research Institute, University of Quebec in Trois-Rivieres (UQTR), 3351 des Forges, Trois-Rivieres G9A 5H7, Canada
[c] Surface Engineering and Nanostructured Materials Research Group, Department of Chemical and Materials Engineering, Complutense University of Madrid (UCM), Av. Complutense, 28040 Madrid, Spain
[d] Department of Materials Physics, Eötvös Loránd University (ELTE), Budapest, P.O.B. 32, H-1518, Hungary
[e] Department of Metallurgical and Materials Engineering, The University of Alabama, Tuscaloosa, AL 35487-0202, USA

ARTICLE INFO

Keywords:
Pin on disk
Hardness
Wear
Tantalum
Severe plastic deformations
Microstructure

ABSTRACT

This article studies the evolution of microstructure and the wear resistance in tantalum processed by a newly developed Severe Plastic Deformation (SPD) technique called Indirect Extrusion Angular Pressing (IEAP). The microstructure and tribological behavior of nanostructured tantalum processed by IEAP were analyzed in this work. The samples were extruded for two, five, and twelve passes of IEAP and then exposed to ball-on-disk wear testing in dry sliding conditions. It was shown that after twelve IEAP passes, an extensive grain refinement down to 500 nm was achieved, hardness increased, and a high dislocation density formed in the material. The wear resistance of the material improved successively after each pass of IEAP, and the wear rate decreased, although the friction coefficient did not change. Evaluation of the morphology of the wear tracks showed that the dominant wear mechanisms were comprised of galling, adhesive wear, pitting and microplowing. Refinement of the microstructure by IEAP led to a reduction in adhesive wear and pitting while a slight increase in oxidation appeared. Comparison of the results of wear testing between tantalum against steel balls and tantalum against alumina balls showed that the presence of alumina generated a larger portion of adhesive wear, making the wear mechanism more complicated while the tantalum-steel pair presented milder wear.

1. Introduction

Tantalum as a refractory metal has served as a biocompatible and high melting point metal within different applications. Interestingly, as a bcc crystal-structured metal, it is ductile at temperatures below 150 °C [1,2]. Tantalum is non-allergenic and therefore can be used in jewelry manufacturing technologies [3]. As a hard blue-grey metal with a density of 16.65 g/cm^3 with high corrosion resistance, it showed different capabilities for a variety of applications such as a chemically resistant material for the production of tanks, valves, and heat exchangers [4], applications in high temperature or severe environment for jet engine components or turbine blades [5–7], capacitors [8,9], as well as biomedical applications as a highly bioinert metal [10,11]. In addition, tantalum coating can enhance the biocompatibility and tribological properties of implant components [12].

As-received tantalum is basically produced by cast vacuum arc remelting (VAR) or electron beam melting (EBM) techniques that make the material highly textured with inhomogeneous microstructure containing large and small grains [13,14]. Modification of such heterogeneous microstructure by conventional techniques was proved to be difficult [15,16]. Severe Plastic Deformations (SPD) particularly by Equal Channel Angular Pressing (ECAP), as evidenced in ref. [17–20], are able to improve the hardness as well as to break down such textured microstructure and refine it homogeneously followed by a recrystallization heat treatment especially when refined-equiaxed grains are expected [14]. Having a very high melting temperature (3020 °C), dynamic recovery at room temperature is almost impossible for tantalum to occur, and therefore, SPD may result in extremely fine

* Corresponding author at: Department of Mechanical and Industrial Engineering, Tallinn University of Technology (TalTech), Ehitajate tee 5, Tallinn 19086, Estonia.
E-mail address: omranpou@uqtr.ca (B.O. Shahreza).

https://doi.org/10.1016/j.ijrmhm.2022.106079
Received 4 October 2022; Received in revised form 21 November 2022; Accepted 5 December 2022
Available online 9 December 2022

microstructure with high hardness in this metal [21].

Based on conventional theory of Archard, increasing the hardness should enhance the wear resistance of the materials and decrease the volumetric wear loss [22]. Former studies made a lot of efforts to explain the effect of SPD on the wear and tribological properties of materials. Nevertheless, the results available in the literature showed controversial findings on enhancing or deteriorating the wear behavior of materials after SPD [23]. According to these studies, the main factors contributing to the enhancement of the wear resistance after SPD are attributed to the small grain size or refined microstructure, and thereby, higher strength and hardness; on the other hand, the reduction of the wear resistance after SPD in some case studies was associated with a number of factors such as lowering the work hardening capability and decreased ductility, higher oxidation rates, and unstable grain boundaries [22].

Earlier studies about tantalum evaluated the effect of SPD on the microstructural refinement and mechanical properties using ECAP [4,14,18], High Pressure Torsion (HPT) [24], and Sliding Friction [1]. However, only a few works studied the effect of SPD on the wear behavior of this material [21,25–27]. Except for our preliminary work in which the ECAP processed tantalum was studied by ball-on-disk wear testing [27], all other studies implemented surface SPD treatment to examine the wear behavior of the superficies microstructure, suggesting that surface treatment could enhance the wear resistance of tantalum in dry sliding condition. Yet, to the best of the authors' knowledge, no comprehensive research has been conducted to investigate the effect of SPD on bulk tantalum and the subsequent effects on the microstructure and wear properties. The aim of this work, therefore, is to understand the effect of SPD processing of bulk tantalum on the microstructure and to evaluate the impact of grain refinement on the wear and tribological behavior. This material, as mentioned above, has a wide range of applications in industry and the control of wear and tribological properties can attract great interest for commercial purposes.

A new SPD technique was exploited here to refine the microstructure of the material in this work. The technique named as Indirect Extrusion Angular Pressing (IEAP) was adapted from the principles of ECAP die. ECAP, in general, is the most frequently used SPD technique [28] while the advantage of using IEAP is that based on the principles of indirect, it can reduce the frictional force between the workpiece and die during the extrusion [29], and therefore, it will be useful for the extrusion of high-strength materials such as tantalum, especially at higher pass numbers when the strength of material increases significantly and hence, increasing the chance of failure of the die or the punch [4,30].

2. Experimental procedure

An IEAP die was employed to process the samples with a square cross section, a channel angle (ϕ) of 90°, and a corner angle (ψ) of 0°, thus, imposing an equivalent Von-Mises strain value of $\varepsilon = 1.155$ during each pass of extrusion. Tantalum ingots composed of Ta $\geq$ 99.5%, Nb $\leq$ 0.3%, Ga $\leq$ 0.1% (all in wt%) supplied by NPM SILMET- Estonia- were prepared with the dimension of 12 × 12 × 130 mm for IEAP processing. Samples were processed for two, five, and twelve passes of IEAP and were designated as Ta2, Ta5, and Ta12, respectively. One sample was used in the as-received condition as a reference. All experiments were conducted at room temperature using route Bc [19]. Molybdenum disulfide (MoS2) was used as a lubricant during the process.

A microhardness tester (model: SHIMADZU HMV-G31, manufacturer: Shimadzu Corporation, Kyoto, Japan) was used for measuring the Vickers hardness (HV) of the specimens with an applied load of 200 g and a dwell time of 15 s. Ten indentations were made along the diameter of each specimen and the average value was considered as the overall result of hardness. At least two samples of each group were tested to assure the reliability of the results. A multi-function tribometer (model: MFT-5000, manufacturer: Rtech Instruments, San Jose, CA, USA) was utilized for the wear tests to carry out the ball-on-disk experiments in dry sliding conditions at ambient temperature. Such type of tests is useful when the surface resistance against abrasion is a key factor in addition to offering the possibility of measuring the ball penetration into the surface [31]. Prior to the wear tests, all samples were mechanically polished to the roughness of Ra = 1 μm and cleaned with acetone. Stainless steel balls are commonly used as a counter body surface in the tribological analysis of materials when the degree of corrosion and toughness of the counter body is not available. In this study, stainless steel balls (AISI 304) were chosen because of the fact that the physical and mechanical properties of tantalum might vary due to the IEAP processing and microstructural refinement. The balls (manufacturer: Redhill Precision Specialty Balls, Prague, Czech Republic) with the chemical composition of C $\leq$ 0.15%, Cr $\approx$ 17–19%, Mn $\leq$ 2.0%, Si $\leq$ 1.00%, S $\leq$ 0.03%, $P \leq$ 0.045%, Ni $\approx$ 8–10%, Fe: balance -all in wt%- with a diameter of $\emptyset$ = 11.1 mm, a surface hardness of 25–39 HRC, and surface roughness of Ra = 0.5 μm were used for ball-on-disk tests. Aluminum oxide ceramics have also shown a great performance in wear and dimensional stability as well as resistance against heat and corrosive atmosphere and therefore, have a wide range of applications in the analysis of wear in industries. For comparison, the results of wear testing against steel balls were compared to those of alumina pair using aluminum oxide ceramic balls (manufacturer: Redhill Precision Specialty Balls, Prague, Czech Republic) with a surface hardness of 1500 HV10, and the chemical composition of $Al_2O_3 \leq$ 99.5%, MgO < 0.2%, and 0.3% other elements, all in wt%.

The balls were gripped firmly in the load arm on top of the specimen, while the specimen had a rotation around its central axis to make a circular wear track on the surface with a diameter of 10 mm. The wear test was performed with a rotational speed of $\omega = 200 \pm 2$ rpm, which corresponds to a relative sliding velocity of ~0.1 m/s between the ball and disk. The measurement of the wear tracks was conducted with the time steps of 30, 120, 300, 900, 1800, and 3000 s for each sample which corresponds to the sliding distance of 3.14, 12.56, 31.4, 94.2, 188.4, and 314 m, respectively. A new ball was employed for each test, and a 1-kgf load was applied normally to the ball which resulted in the maximum Hertzian contact pressure of 0.88 GPa in this tribosystem. All ball-on-disk tests were conducted based on ASTM-G99 standards [32], and the effect of IEAP processing on the wear resistance of the material was studied. All the tests were repeated three times to ensure the repeatability and reproducibility of the results. A non-contact 3D confocal microscope (model: Bruker Contour GT- K0+ optical profilometer, manufacturer: Bruker Corporation, Billerica, MA, USA) with a vertical resolution of 0.01nm and a lateral resolution of 0.38μm was used to measure the depth of the wear track and the wear rate of materials. Six separate sections with dimensions of 320 × 1300 μm in each wear track were selected and scanned by the 3D profiler, and the total volumetric wear loss (hereinafter volume loss) and the wear rate were measured by considering the total length of the wear track. Morphologies of the worn surface were examined by using an optical microscope (Nikon Epiphot 200), and a Scanning Electron Microscope (model: Bruker Esprit 1.8, manufacturer: Bruker Corporation, Billerica, MA, USA). The composition of worn surfaces was studied by an EDAX spectroscopy running at 20 kV in the same electron microscope.

For the microstructural analysis of the samples, they were mechanically polished with SiC abrasive papers of 1200, 2500, and 4000 grit, and then polished with aluminum oxide suspensions of 5, 3, and 1 μm powders, consecutively. In the final step, the surface was polished by a colloidal silica suspension (OP-S) with a particle size of 40 nm, and for the X-ray diffraction study, the surface was etched with HNO_3:HF:H_2O. The evolution of microstructure was investigated by electron backscatter diffraction (EBSD) using an SEM instrument (model: FEI Quanta 3D, manufacturer: Thermo Fisher Scientific, Waltham, MA, USA). The step size was about 30 nm, and Orientation Imaging Microscopy (OIM) software was used for the analysis of EBSD images. In order to differentiate between the low-angle boundaries (LAGBs) and high-angle boundaries (HAGBs), a 15° criterion was employed for the misorientation angle.

The crystallite size and the dislocation density were determined by X-ray line profile analysis (XLPA). The measurement of the diffraction peaks was conducted using an RA-MultiMax9 rotating anode diffractometer (model: RA-MultiMax9, manufacturer: Rigaku, Tokyo, Japan). The wavelength of the applied CuKα_1 radiation was 0.15406 nm. The evaluation of the diffraction patterns was performed by the Convolutional Multiple Whole Profile (CMWP) fitting method [33]. During this procedure, all diffraction profiles in the pattern were fitted simultaneously by the convolution of measured instrumental peaks and theoretical profiles calculated for crystallite size and dislocation broadening. The CMWP fitting yielded the area-weighted mean crystallite size ($<x>_{area}$) and the dislocation density (ρ). $<x>_{area}$ was obtained from the median (m) and the square root of the lognormal variance (σ) of the crystallite size distribution as $<x>_{area} = m \times \exp.(2.5\,\sigma^2)$. The CMWP evaluation procedure requires the dislocation contrast factor values which can be calculated from the anisotropic elastic constants of the crystal. The values of the elastic constants c_{11}, c_{12} and c_{44} are 262, 157, and 82 GPa, respectively, for Ta [34]. Using ANIZC program [35] the values of $\overline{C}_{h00}$ for edge and screw dislocations were calculated as 0.201 and 0.263, respectively.

3. Results

3.1. Microstructure and hardness

Using the CMWP fitting technique, the theoretical patterns were fitted to the experimental diffractograms, and the dislocation density and crystallite size for each sample were measured. For example, Fig. 1 shows the CMWP fitting for the sample processed by twelve passes of IEAP.

Fig. 2-a shows an SEM image of the coarse-grained (CG) microstructure obtained from the as-received specimen. The average grain size of the initial sample was ~11 μm. Images in Fig. 2b-g present the EBSD crystallographic orientation (Inverse Pole Figure, IPF) and grain maps for the specimens processed by two (b,c), five (d,e) and twelve (f,g) passes of IEAP. The size of grains was defined as the volume bounded by boundaries with misorientation angles higher than 15^0. The initial grain size of ~11 μm was reduced to ~4.7 μm after two passes of IEAP, and

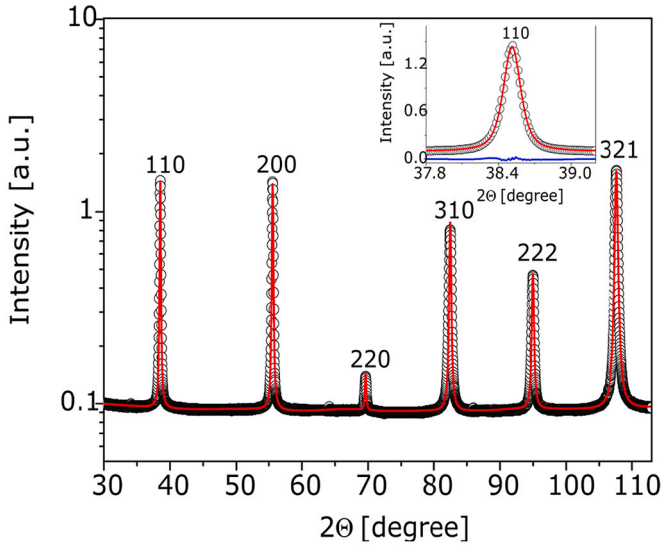

Fig. 1. CMWP fitting on a specimen after twelve passes of IEAP. The open circles and the solid line represent the measured data and the fitted pattern, respectively. The intensity was plotted on a logarithmic scale. The inset shows a part of the diffractogram with higher magnification on a linear intensity scale. The difference between the measured and the fitted patterns is shown at the bottom of the inset.

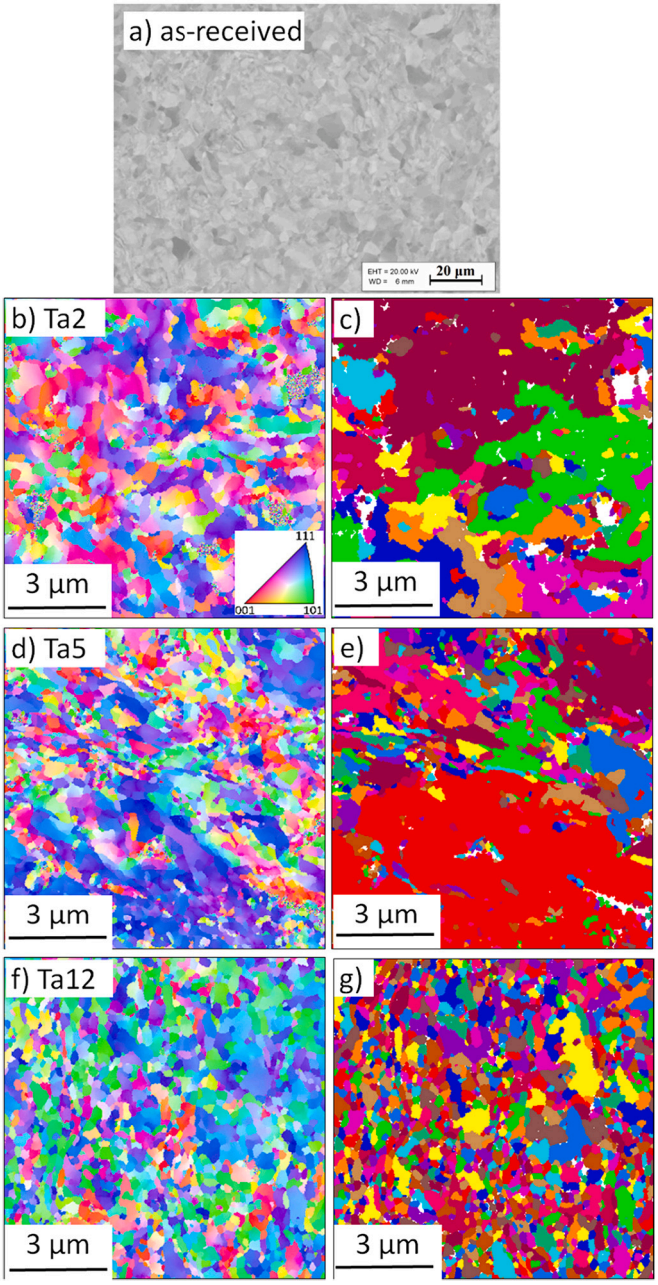

Fig. 2. SEM image showing the initial CG microstructure (a), and EBSD crystallographic orientation (b,d,f) and grain maps (c,e,g) for the IEAP processed specimens.

eventually decreased to ~500 nm after twelve passes. The average grain size values obtained by SEM/EBSD are listed in Table 1.

The grain size and the misorientation angle distribution determined by the EBSD images for the IEAP processed samples are shown in Fig. 3. For two and five passes, bimodal grain size distributions were detected. Namely, for two IEAP passes ~40% of the grains have a large size of about 10 μm while ~60% have a size below 3 μm. For five passes, both fractions were slightly refined. After twelve passes, large grains were not found and the distribution became monomodal as shown in Fig. 3e. Regarding the misorientation-angle distribution, a very high LAGB fraction was observed after two passes since the dislocations multiplicated during IEAP can form LAGBs. By increasing the number of passes, the HAGB fraction increased in accordance with the grain refinement.

The crystallite size and the dislocation density determined by XLPA

Table 1
Structural parameters of tantalum samples before and after IEAP processing. The area-weighted mean crystallite size ($<x>_{area}$) and the dislocation density (ρ) were calculated by XLPA; the grain size (D_{area}) and the HAGB fraction (V_{HAB}) were measured by EBSD.

Sample	*Equivalent von-Mises strain*	D_{area} [μm]	$<x>_{area}$ [nm]	ρ [10^{14} m^{-2}]	V_{HAB} %	*Microhardness [HV0.02]*
as-received	–	11 ± 1	800 <	< 0.1	–	105 ± 10
Ta 2	2.31	4.7 ± 0.7	425 ± 59	2.2 ± 0.3	33	184 ± 8
Ta 5	5.78	3.5 ± 0.5	149 ± 21	7 ± 1	41	211 ± 11
Ta 12	13.86	0.5 ± 0.1	52 ± 7	18 ± 2	68	243 ± 7

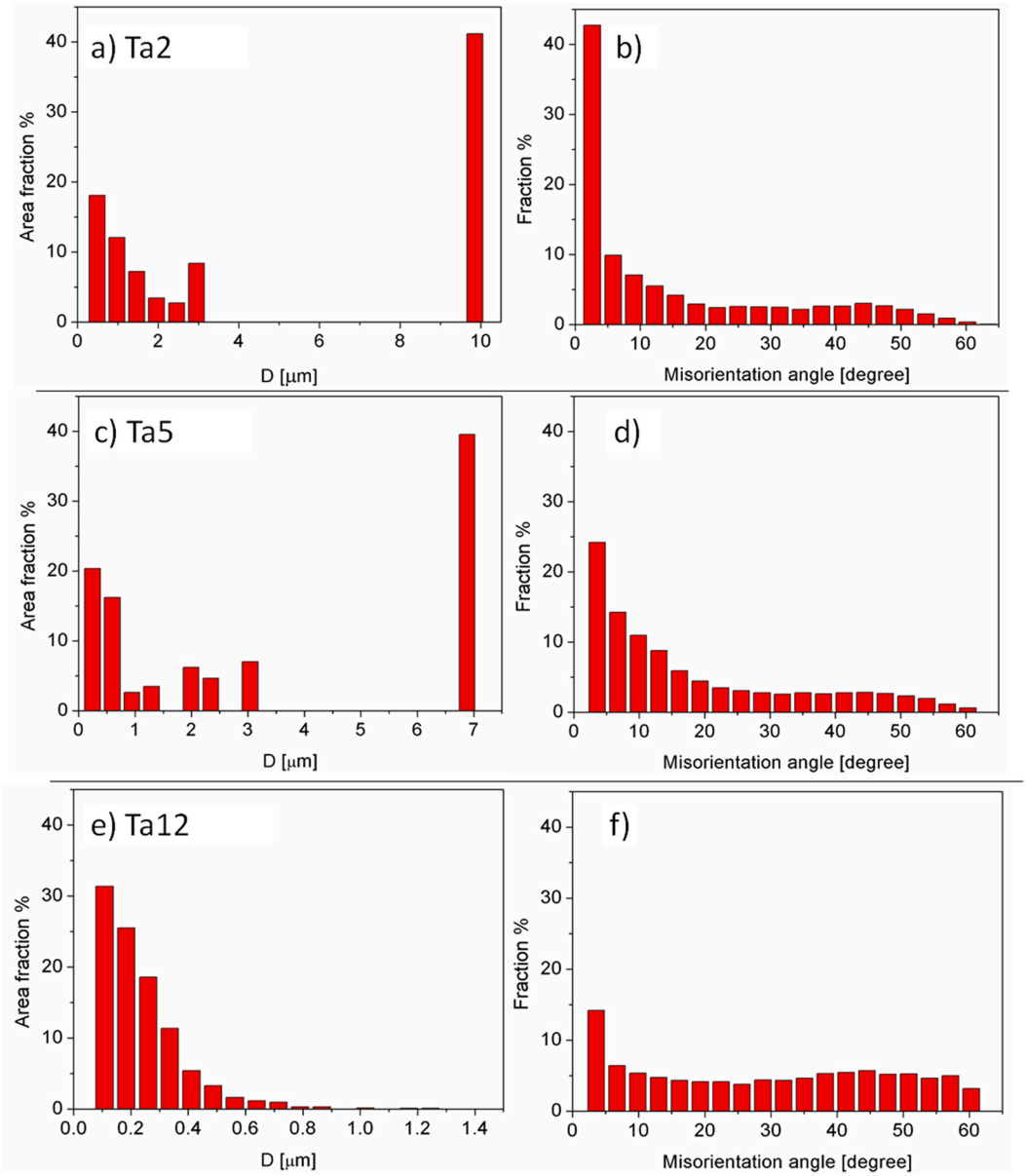

Fig. 3. Distribution of grain size (left) and grain-boundary misorientation angles (right) for the specimens processed for two (a,b), five (c,d), and twelve (e,f) passes of IEAP.

are listed in Table 1. After two passes of IEAP, the crystallite size and dislocation density were measured as ~425 nm and ~ 2.2 × 10^{14} m^{-2}, respectively. It is noted that the crystallite size in metallic materials obtained by XLPA is basically smaller than the grain size measured by electron microscopy. This discrepancy can be explained by referring to the fact that the crystallite size is defined as the volume that scatters the X-ray beams coherently, and the lattice dislocations inside the grains can break the coherency of the X-ray beams. These volumes are sometimes named as "subgrains" and are relatively smaller than the grain size values observed by electron microscopy techniques [29]. The results obtained here show that increasing the number of IEAP passes decreased the crystallite size and increased the dislocation density, and their corresponding values reached about 52 nm and 18 × 10^{14} m^{-2}, respectively, after twelve passes of IEAP. Structural parameters of the samples

as well as the hardness and the equivalent imposed strain for each sample are summarized in Table 1.

3.2. Ball-on-disk tests

3.2.1. Wear behavior

Fig. 4 shows the coefficient of friction (COF) of a tribosystem of steel-tantalum pair (a tantalum disk rotating under a loaded steel ball) in dry sliding conditions for 3000 s. These results show that the microstructural refinement of the material did not have a significant impact on the COF. All specimens presented a COF ranging between 0.36 and 0.43.

Investigations on the volume loss and specific wear rate were conducted on the wear tracks by implementing confocal microscopy. Fig. 5 exemplifies the 3D profile and 2D cross section of the wear track in the as-received sample. Taking into account the two algebraic values of positive volume (P·V) and negative volume (N·V) measured by the confocal microscope, the two parameters of displaced volume (D·V) and volume loss (V.L) can be defined as:

$$Displaced\ volume = |N.V| + |P.V| \quad (1)$$

$$\text{Volume loss} = |N.V| - |P.V| \quad (2)$$

As such, displaced volume is the sum of absolute values of the P·V and N·V, and volume loss is the difference between the absolute values of the two parameters [36].

By considering the whole wear track in each sample, the amount of volume loss and specific wear rate (the volume loss per distance per normal load) [37] were obtained and plotted in Fig. 6. These graphs show that IEAP had a noticeable effect on the enhancement of the wear resistance of materials. For the total wear-test time of 3000 s, the volume loss and wear rate decreased by ~35%, just after two passes of IEAP, and eventually, decreased by 58% after twelve passes as compared to the initial values before IEAP. It should be noted that the wear rate at the beginning of the test (up to 300 s) was unstable in all samples, then it approached a steady-state rate showing a downward trend.

3.2.2. Morphology of wear tracks

In order to understand the effect of IEAP on the wear behavior of tantalum and subsequent impacts on the wear mechanisms, optical and SEM microscopy observations on the wear tracks are provided below.

Fig. 7 shows the optical microscope images of the surface of the wear tracks, demonstrating the transition of the wear within different time intervals during the wear test. In both cases of the as-received and processed samples (Ta12), the effects of abrasive and adhesive wear are visible.

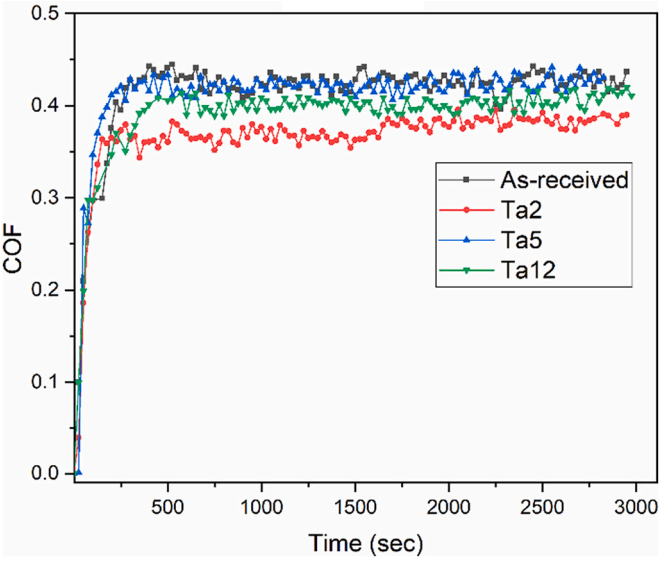

Fig. 4. COF of as-received and processed specimens using a steel ball. The uncertainty is <6%.

SEM investigations of the wear tracks were conducted and provided in Fig. 8 to further analyze and compare the wear mechanisms after accomplishing the test in the unprocessed (as-received) and IEAP-processed samples. Several wear mechanisms are discernible in the samples. Abrasive wear in the form of microplowing and the presence of ridges and grooves can be found in all cases. Adhesive wear in the form of galling and smearing of materials on the surface and built-up edges at the corners of the wear tracks can also be noticed in the samples. Fatigue wear in the form of pitting and the appearance of small cavities is another predominant mechanism of wear that is found mainly in the as-received sample. This type of wear is the result of repetitive loading and the subsequent initiation and propagation of microcracks on the surface or sub-surface of the samples which finally leads to the separation of materials.

Furthermore, the results of EDS analysis on the surface of the wear tracks (Fig. 9 & Table 2) confirmed the oxidative wear in the as-received and IEAP-processed samples.

The presence of iron and chromium on the surface of the wear track indicates the traces of material transfer from the steel ball to the workpiece during the wear test. This transfer mainly occurred in the galling and smearing zones where the materials rigidly adhered to the surface. Galling and smearing are two types of severe adhesive wear that usually happen in unlubricated materials leading to surface roughening and the appearance of protrusions [38]. As a result of roughening and severe adhesive wear, galling comes along with a rise in the temperature and thereby, oxidation of the surface.

4. Discussion

The effect of SPD processing on tantalum has been evaluated in several studies in the literature. The main focus of these studies was mainly narrowed to the microstructure and mechanical properties, and less attention was dedicated to the wear and tribological behavior of the material. These results unanimously acknowledged that applying SPD and imposing plastic strains enhanced the strength of the material. Such enhancement is attributed to two factors: Grain refinement and accumulation of dislocation densities [39]. In addition to SPD techniques, other cold working methods such as micro-coining also proved the effect of accumulation of dislocation densities (up to 10^{13}–10^{15} m^{-2}) on the hardness of tantalum [40].

Depending on the amount of strain, however, the contribution of grain refinement or dislocation densities might be different. A comprehensive study on HPT processing of Ta and Nb showed that work hardening above the strain values of $\varepsilon_{vm} \approx 7$ will not significantly affect the grain size while the dislocation densities can increase monotonously [24]. This statement is in agreement with the results of the present study. As illustrated in Fig. 10, by increasing the strain, at first the grain size decreased quickly and then, leveled off from the original trend. On the other hand, the dislocation density demonstrated rather linear growth by increasing the amount of strain.

The friction of metallic materials in dry sliding conditions is usually high due to plastic deformation, abrasion, and delamination [25]. The present study showed that SPD processing of tantalum by IEAP could improve the wear resistance of the material by means of increasing the hardness and consequently, decreasing the volume loss of the material, though the coefficient of friction (COF) did not change significantly and only varied between 0.36 and 0.43; see Fig. 4 & Fig. 6. A similar study on the wear testing of surface-SPD processed tantalum against steel balls also reported an enhancement in the wear resistance of the material, as well as a similar range of COF [25]. Former studies about the effect of SPD on the COF, however, presented controversial results. For instance, recent studies on titanium showed a reduction in COF [41,42], while another work reported a reverse effect [43]. Nonetheless, the main

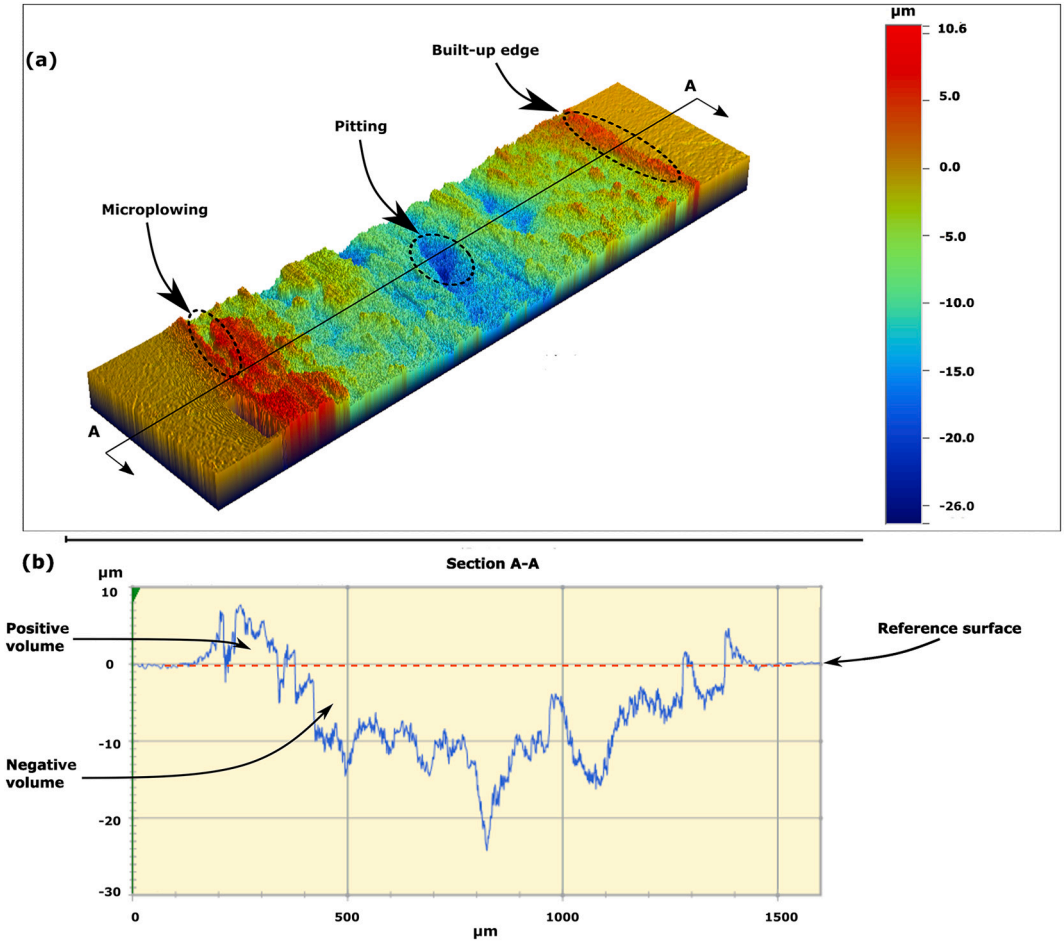

Fig. 5. Confocal microscopy observation of the wear track for the as-received sample; (a) 3D profile of the wear track; (b) 2D profile of the A-A section demonstrating the positive displaced volume and negative displaced volume located above and below the red-dash line, respectively. (For interpretation of the references to colour in this figure legend, the reader is referred to the web version of this article.)

outcome of these studies is that COF could be influenced by several factors such as the load scale when varying from nano to macro level. Further, the reason for the fluctuation of this parameter is mainly because of the inhomogeneity of the SPD-induced microstructure along the sliding route [42].

Results of mechanical testing showed that IEAP improved the hardness and wear resistance of tantalum due to the microstructural refinement, and each further pass of IEAP helped to improve this enhancement. As demonstrated in Fig. 11, increasing the imposed strain (further passes of IEAP) increased the hardness and reduced the volume loss and hence enhanced the mechanical properties of the material.

Yet, the results of our earlier study on tantalum processed by the same IEAP die but using alumina balls as the counter-body wear surface showed no enhancement in the wear as well as the appearance of different wear mechanisms [27]. To comprehend this difference, the two experiments are evaluated in three different aspects as follows:

- 1) The worn surface of the balls: A detailed observation of the worn surface of the balls in these two experiments may help to understand this difference better. Fig. 12 illustrates the surface of the steel ball where the worn area and fine particles of debris can be found on the surface.

Results of the EDS analysis (Table 3) show that a small portion of debris on the steel ball contains tantalum (7 to 18 wt%), and the main parts are worn particles of iron that are detached from the steel ball itself and adhered back. On the contrary, the EDS analysis of the surface of the alumina balls obtained from the previous work [27], revealed that a larger portion of tantalum debris (41 to 44 wt%) was found on the surface of the ball, implying this fact that tantalum tends to stick to the surface of the alumina ball, and the rate of materials transfer is higher as compared with the case of using steel balls.

- 2) The wear tracks on the specimens: As explained in Section 3.2.1, the appearance of positive displaced volume (P·V) and higher ratios of positive volume to the total displaced volume (D·V) is an indication of adhesive wear when materials are removed from the wear track and pushed away from the grooves to be accumulated in the form of hills. Soft materials such as pure aluminum and pure niobium usually display this behavior when exposed to dry-sliding wear [44,45]. On the other hand, decreasing the amount of P·V and the ratio of $\frac{P.V}{D.V}$ as a whole, could be an indication of the reduction of adhesive wear [36]. This proposed ratio could also demonstrate the capacity of the material for plastic deformation during wear. Table 4 compares this ratio in the wear tracks of the two experiments.

As shown in Table 4, by increasing the number of IEAP passes, the ratio of P·V/D·V in the wear tracks of the tantalum-steel pair is constantly decreasing (as the result of increasing the hardness); but in the case of the tantalum-alumina pair, this ratio is higher and there is no decreasing trend even after twelve passes of IEAP extrusions. This fact implies that when using alumina balls against tantalum, the tendency for materials transfer (rather than materials removal) is higher, and increasing the hardness had no effect on it.

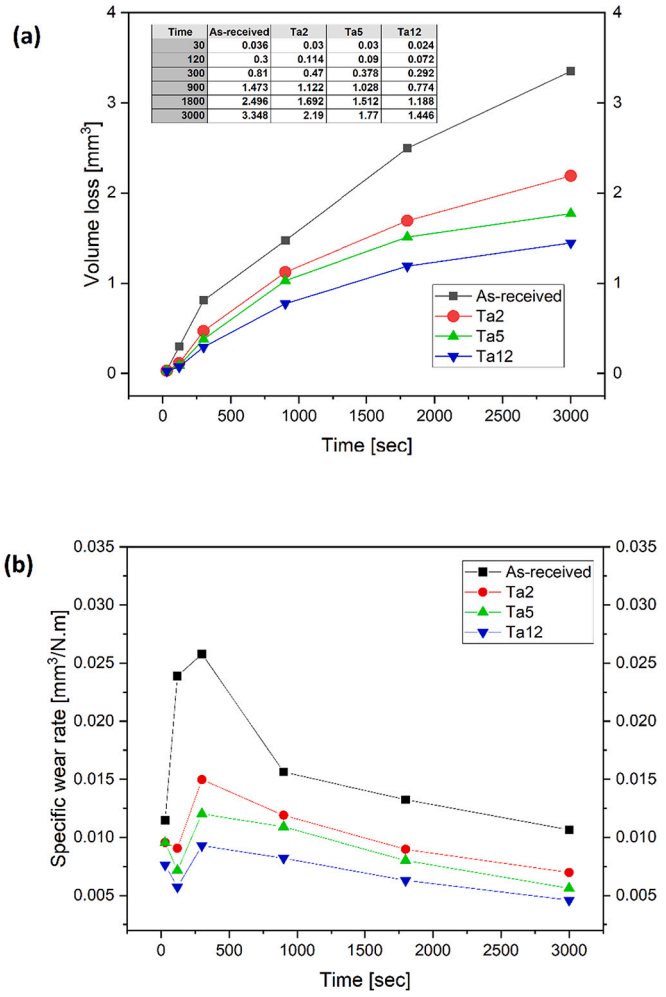

Fig. 6. The influence of sliding time and IEAP pass numbers on the wear behavior of tantalum: (a) volume loss; (b) specific wear rate. The relative error is <13%.

- 3) The combined mutual effect of counter-bodies on the tribosystem and the friction coefficient (COF): Results of experiments showed that COF between tantalum and steel balls was lower (0.36–0.43) than that of alumina balls (0.5–1.0). Generally, lower adhesive wear results in lower COF in metals [42].

The aforementioned arguments suggest that tantalum has a tendency for adhesive wear when paired with alumina balls and the rate of materials transfer is higher compared to that of steel balls. Similar studies evaluating the effect of counter-body of tantalum in a tribosystem also showed the occurrence of materials transfer when it is paired with titanium or titanium alloys, and accordingly, the appearance of adhesive wear and micro-welding even at high-velocity sliding (34 m/s) [46,47]. In general, adhesive wear is a common type of wear that could appear in soft and ductile materials [48], making a great contribution to forming the positive displaced volume in the wear. As a result, despite the Archard theory, there might be some cases when the hardness increases after SPD, but the counter-body surface exerts the adhesive wear and minimizes the effect of hardness.

It is also worth noting that the tribological behavior of a tribosystem is not a property of the material, since the response to the external stresses influences the whole system [23]. As can be seen here, changing the counter-body of the tribosystem noticeably affected the wear mechanisms and COF in materials. Nevertheless, it can be concluded that SPD processing of tantalum can improve the hardness and wear resistance of the material. Yet, to prevent the occurrence of severe adhesive wear and appearing the complexity in the wear, it is suggested to avoid the use of titanium or alumina as a counter-body surface.

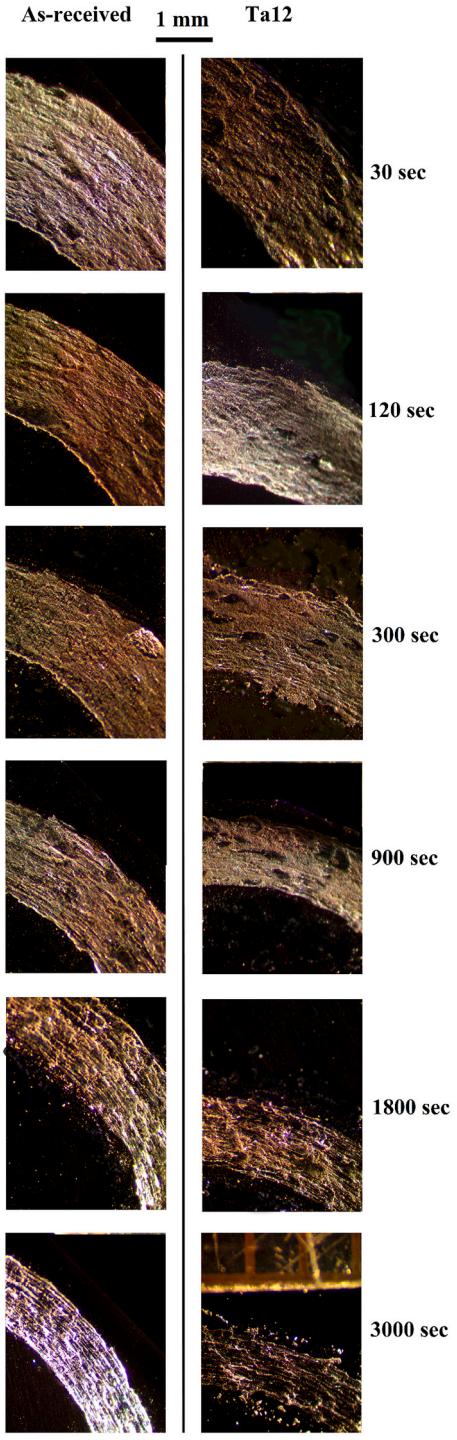

Fig. 7. Optical microscope images of the wear tracks in as-received and Ta12 specimens in different time slots of wear testing.

5. Conclusions

In this research, the effect of a modern SPD technique called IEAP on the tribological properties of nanostructured tantalum was investigated. Tantalum (Ta) samples with a purity of ~99.5 wt% were processed by IEAP for two, five, and twelve passes, and the microstructural

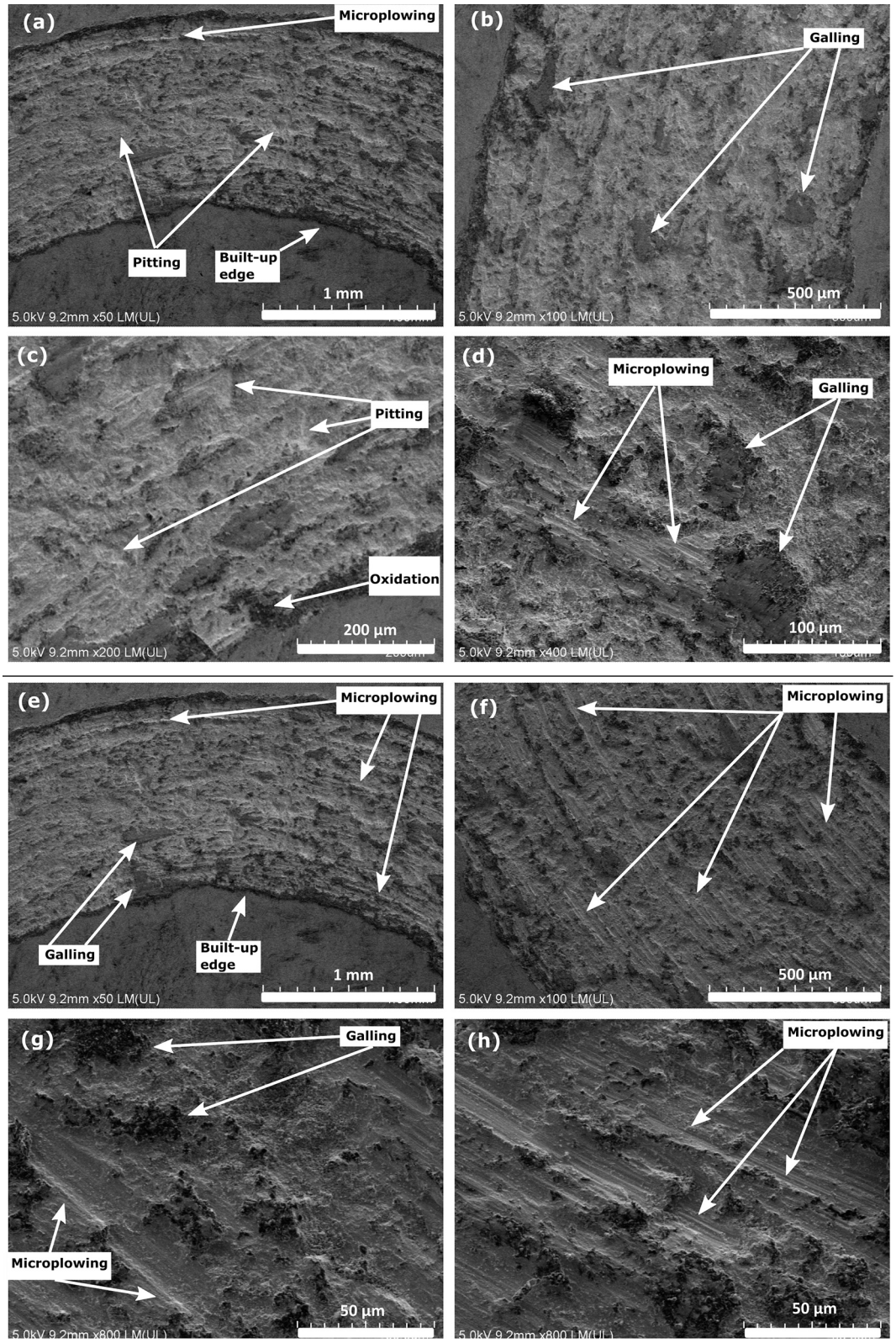

Fig. 8. SEM investigations of the morphology of the wear track on the unprocessed sample with CG microstructure (a, b, c, and d) and IEAP-processed sample (Ta12) with UFG microstructure (e, f, g, and h).

refinement and the following impacts on the hardness and wear behavior of the material were tested. Based on the results, the following conclusions are drawn:

- Substantial microstructural refinement was obtained after twelve passes of IEAP extrusions. The as-received grain size of ~11 µm was reduced to ~500 nm. Evaluation of the microstructure using X-ray line profile analysis also showed that high densities of dislocations up to 18×10^{14} m^{-2} were induced in the material.

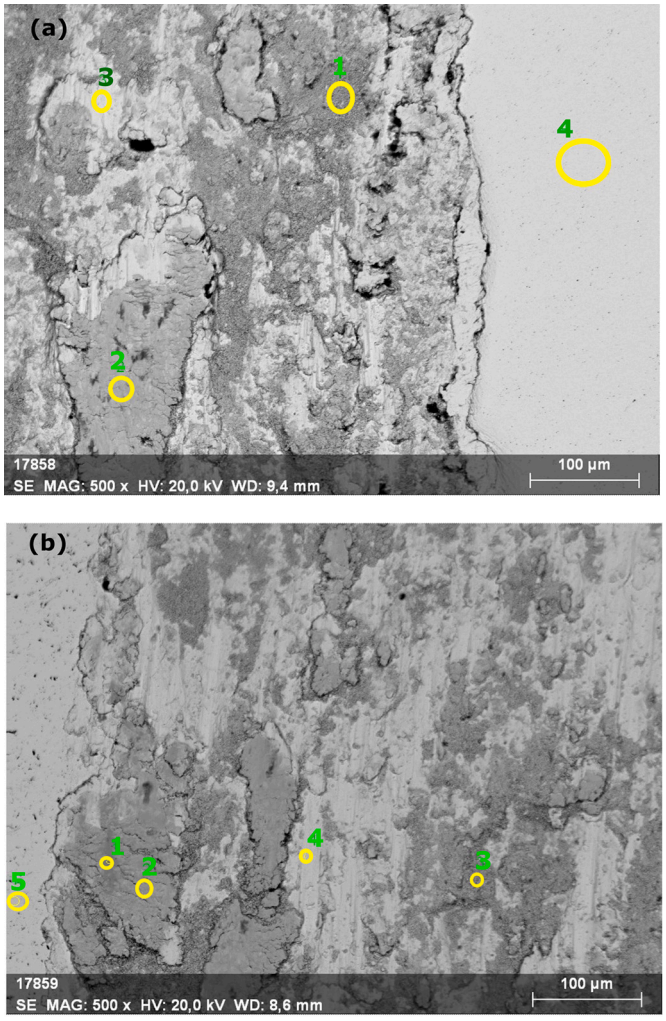

Fig. 9. SEM-EDS investigations of the wear tracks in as-received (a) and Ta12 (b) samples as well as the corresponding selected areas for EDS analysis: (a). The selected areas in the as-received sample were taken from (1) galling, (2) smearing, (3) pitting, and (4) Intact area -out of wear track. The selected areas in Ta12 were taken from (1), (2)& (3) galling, (4) microplowing, and (5) intact area.

Table 2
Results of EDS analysis of the wear tracks in as-received and IEAP-processed samples. The spectrum numbers describe the location of the study in Fig. 9.

Sample	unn. C [wt%]					
		Tantalum	Oxygen	Iron	Chromium	Nb
As-received	Spectrum 1	81.36	14.47	3.19	0.99	0.31
	Spectrum 2	80.16	12.75	3.42	0.97	0.36
	Spectrum 3	96.53	0.35	0.78	–	0.20
	Spectrum 4	98.11	–	–	–	0.29
Ta12	Spectrum 1	67.19	24.80	4.96	1.73	0.27
	Spectrum 2	63.64	28.14	4.11	1.47	0.29
	Spectrum 3	72.04	18.78	4.57	0.94	0.13
	Spectrum 4	93.65	–	1.91	–	0.23
	Spectrum 5	97.42	–	–	–	0.40

- The hardness of the material increased by 2.3 times the original value; the initial hardness of 105 HV increased to 243 HV after twelve passes of IEAP.
- Results of wear tests showed that IEAP improved the wear resistance of Ta since the volume loss and the wear rate decreased by 58% after twelve passes of IEAP, although no significant change in the coefficient of friction was observed.
- A new parametric ratio (positive displaced volume to total displaced volume; P·V/D·V) based upon the 3D profilometry of the wear tracks was defined to estimate the transition of the wear mechanism from abrasive wear to adhesive wear and vice versa. This parameter could also represent the capacity of the material to undergo plastic deformation during wear testing.
- The wear mechanism in the initial sample was comprised of adhesive wear, plowing on microscopic scales (microplowing), pitting, and galling, while after twelve passes of extrusion, the dominant wear mechanisms were microplowing, oxidation, and galling. In brief, IEAP processing improved the wear resistance of Ta, and the wear turned out to be milder, though a slight increase in oxidation as a result of increasing the hardness appeared.
- Evaluation of the effect of the counter-body surface on the wear testing of tantalum revealed that the selection of the counter-body surface against the target material is important and should be considered in the analysis of the wear and tribological properties.

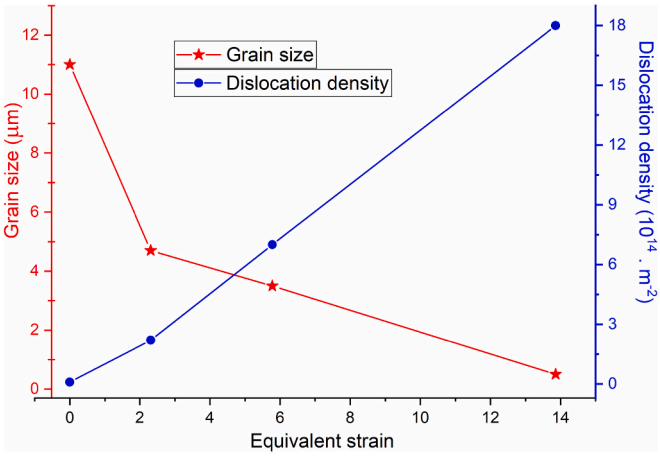

Fig. 10. Evolution of structural parameters in tantalum with respect to the induced strain. The red axis on the left side shows the grain size, and the blue axis on the right side represents the dislocation density. The relative error is <14%. (For interpretation of the references to colour in this figure legend, the reader is referred to the web version of this article.)

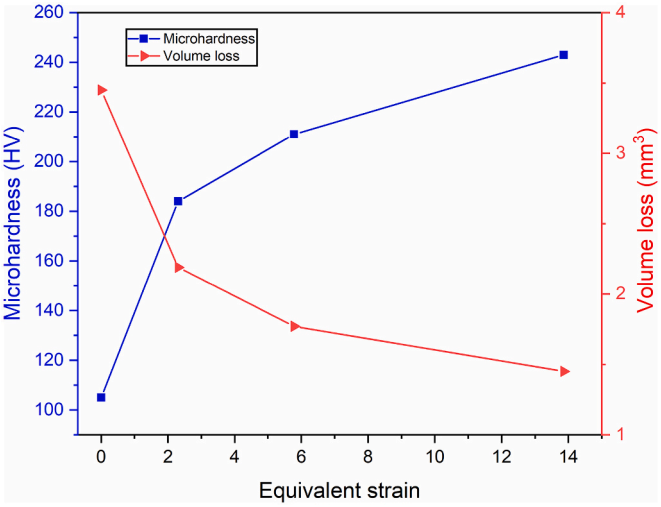

Fig. 11. Evolution of microhardness and volume loss in tantalum with respect to the induced strain. The volume loss was measured after running the wear test for 3000 s. The relative error is <12%.

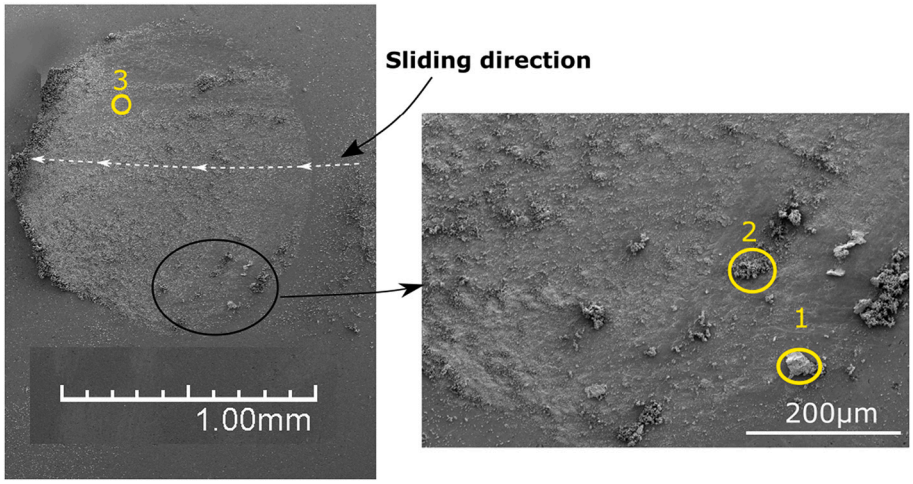

Fig. 12. SEM analysis of the worn surface of the steel ball after running the wear test against tantalum (Ta12). Numbered circles refer to the selected areas for EDS analysis.

Table 3
Analysis of the chemical composition on the surface of the steel ball. The spectra refer to the circles indicated in Fig. 12.

unn. C [wt%]					
	Tantalum	Oxygen	Iron	Chromium	Carbon
Spectrum 1	9.56	0.86	83.19	1.19	0.99
Spectrum 2	18.16	10.25	63.42	0.70	1.26
Spectrum 3	7.53	6.35	79.78	1.00	0.10

Table 4
The ratio of positive volume (P·V) to total displaced volume (D·V) in wear tracks of tantalum when paired with steel balls and alumina balls. The results of the alumina ball were extracted from the previously published work [27].

	P·V/ D·V (%)			
Tribosystem	As-received	Ta2	Ta5	Ta12
Tantalum- Alumina	8	10	7	7
Tantalum-Steel	7	5	5	3

When using steel balls, tantalum presented lower friction and lower transfer of materials, whereas using alumina balls, the same material showed a tendency for adhesive wear and materials transfer. Therefore, when paired with the alumina ball, tantalum could not present a noticeable change in the wear resistance before or after SPD processing due to the material transfer and complexity of the wear.

Credit author statement

Conceptualization: B·O. Shahreza and L. Kommel, Methodology: B. O. Shahreza, M. Antonov, L. Kommel, J. Huot, A. Heczel Data curation: B.O. Shahreza, F. Sergejev, J. Huot Experimental investigations: B.O. Shahreza, L. Kommel, A. Heczel, M. Antonov, J. Gubicza Supervision of findings: B.O. Shahreza, F. Sergejev, F.J.P Trujillo, and J. Gubicza, Writing the original draft: B.O Shahreza, Funding acquisition: B.O. Shahreza, F.J.P Trujillo, M. Antonov, and F. Sergejev, Review and editing: All authors contributed to the revision and provided critical feedback.

Declaration of Competing Interest

The authors declare that they have no known competing financial interests or personal relationships that could have appeared to influence the work reported in this paper.

Data availability

Data will be made available on request.

Acknowledgment

This research was sponsored by the Estonian Research Council (Grant No. PUTJD1010), and in part by the European Union's Horizon 2020 program, MSCA grant No 847635. M. Antonov would like to acknowledge the support from the Estonian Ministry of Education and Research, and Estonian Science Foundation (M-ERA.NET "DuplexCer", PRG 643).

References

[1] Y.S. Zhang, L.C. Zhang, H.Z. Niu, X.F. Bai, S. Yu, X.Q. Ma, Z.T. Yu, Deformation twinning and localized amorphization in nanocrystalline tantalum induced by sliding friction, Mater. Lett. 127 (2014) 4–7, https://doi.org/10.1016/j.matlet.2014.04.079.
[2] A.A. Navid, A.M. Hodge, Nanostructured alpha and beta tantalum formation—relationship between plasma parameters and microstructure, Mater. Sci. Eng. A 536 (2012) 49–56, https://doi.org/10.1016/J.MSEA.2011.12.017.
[3] R. Grill, A. Gnadenberger, Niobium as mint metal: production–properties–processing, Int. J. Refract. Met. Hard Mater. 24 (2006) 275–282, https://doi.org/10.1016/J.IJRMHM.2005.10.008.
[4] L. Kommel, B.O. Shahreza, V. Mikli, Microstructure and physical-mechanical properties evolution of pure tantalum processed with hard cyclic viscoplastic deformation, Int. J. Refract. Met. Hard Mater. 83 (2019), 104983, https://doi.org/10.1016/J.IJRMHM.2019.104983.
[5] J. Belan, L. Kucharikova, A. Vasko, E. Tillova, The influence of high temperature on DV-2 jet engine Ni-based superalloy turbine blade degradation, in: Mater. Today Proc, Elsevier, 2017, pp. 5743–5748, https://doi.org/10.1016/j.matpr.2017.06.039.
[6] E.J. Pickering, K.A. Christofidou, H.J. Stone, N.G. Jones, On the design and feasibility of tantalum-base superalloys, J. Alloys Compd. 804 (2019) 314–321, https://doi.org/10.1016/j.jallcom.2019.07.003.
[7] C. Booth-Morrison, R.D. Noebe, D.N. Seidman, Effects of tantalum on the temporal evolution of a model Ni-Al-Cr superalloy during phase decomposition, Acta Mater. 57 (2009) 909–920, https://doi.org/10.1016/j.actamat.2008.10.029.
[8] T. Balaji, R. Govindaiah, M.K. Sharma, Y. Purushotham, A. Kumar, T.L. Prakash, Sintering and electrical properties of tantalum anodes for capacitor applications, Mater. Lett. 56 (2002) 560–563, https://doi.org/10.1016/S0167-577X(02)00552-9.
[9] A. Rouahi, F. Challali, I. Dakhlaoui, C. Vallée, S. Salimy, F. Jomni, B. Yangui, M. P. Besland, A. Goullet, A. Sylvestre, Structural and dielectric characterization of sputtered tantalum titanium oxide thin films for high temperature capacitor applications, Thin Solid Films 606 (2016) 127–132, https://doi.org/10.1016/j.tsf.2016.03.047.
[10] T. Beline, J.H.D. da Silva, A.O. Matos, N.F. Azevedo Neto, A.B. de Almeida, F. H. Nociti Júnior, D.M.G. Leite, E.C. Rangel, V.A.R. Barão, Tailoring the synthesis of tantalum-based thin films for biomedical application: characterization and

biological response, Mater. Sci. Eng. C. 101 (2019) 111–119, https://doi.org/10.1016/j.msec.2019.03.072.
[11] A.C. Hee, Y. Zhao, S.S. Jamali, A. Bendavid, P.J. Martin, H. Guo, Characterization of tantalum and tantalum nitride films on Ti6Al4V substrate prepared by filtered cathodic vacuum arc deposition for biomedical applications, Surf. Coat. Technol. 365 (2019) 24–32, https://doi.org/10.1016/j.surfcoat.2018.05.007.
[12] L. Kunčická, R. Kocich, T.C. Lowe, Advances in metals and alloys for joint replacement, Prog. Mater. Sci. 88 (2017) 232–280, https://doi.org/10.1016/j.pmatsci.2017.04.002.
[13] J.B. Clark, R.K. Garrett, T.L. Jungling, R.A. Vandermeer, C.L. Vold, Effect of processing variables on texture and texture gradients in tantalum, Metall. Trans. A 1991 229 (22) (1991) 2039–2048, https://doi.org/10.1007/BF02669871.
[14] S.N. Mathaudhu, K.T. Hartwig, Processing microstructure property relationships in severely deformed tantalum, Mater. Sci. Eng. A 463 (2007) 94–100, https://doi.org/10.1016/J.MSEA.2006.08.120.
[15] J.B. Clark, R.K. Garrett, T.L. Jungling, R.I. Asfahani, Influence of initial ingot breakdown on the microstructural and textural development of high-purity tantalum, Metall. Trans. A. 22 (1991) 2959–2968, https://doi.org/10.1007/BF02650255.
[16] C.L. Briant, E. MacDonald, R.W. Balliett, T. Luong, Recrystallization textures in tantalum sheet and wire, Int. J. Refract. Met. Hard Mater. 18 (2000) 1–8, https://doi.org/10.1016/S0263-4368(99)00028-1.
[17] R.Z. Valiev, A.V. Korznikov, R.R. Mulyukov, Structure and properties of ultrafine-grained materials produced by severe plastic deformation, Mater. Sci. Eng. A 168 (1993) 141–148, https://doi.org/10.1016/0921-5093(93)90717-S.
[18] Q. Wei, T. Jiao, S.N. Mathaudhu, E. Ma, K.T. Hartwig, K.T. Ramesh, Microstructure and mechanical properties of tantalum after equal channel angular extrusion (ECAE), Mater. Sci. Eng. A 358 (2003) 266–272, https://doi.org/10.1016/S0921-5093(03)00305-8.
[19] F. Djavanroodi, B. Omranpour, M. Ebrahimi, M. Sedighi, Designing of ECAP parameters based on strain distribution uniformity, Prog. Nat. Sci. Mater. Int. 22 (2012) 452–460, https://doi.org/10.1016/j.pnsc.2012.08.001.
[20] L. Kommel, J. Huot, B.O. Shahreza, Effect of hard cyclic viscoplastic deformation on the microstructure , mechanical properties , and electrical conductivity of Cu-Cr alloy, J. Mater. Eng. Perform. (2022), https://doi.org/10.1007/s11665-022-06997-w.
[21] Y.S. Zhang, Q.M. Wei, H.Z. Niu, Y.S. Li, C. Chen, Z.T. Yu, X.F. Bai, P.X. Zhang, Formation of nanocrystalline structure in tantalum by sliding friction treatment, Int. J. Refract. Met. Hard Mater. 45 (2014) 71–75, https://doi.org/10.1016/J.IJRMHM.2014.03.011.
[22] N. Gao, C.T. Wang, R.J.K. Wood, T.G. Langdon, Tribological properties of ultrafine-grained materials processed by severe plastic deformation, J. Mater. Sci. 47 (2012) 4779–4797, https://doi.org/10.1007/s10853-011-6231-z.
[23] I. Sabirov, N.A. Enikeev, M.Y. Murashkin, R.Z. Valiev, Multifunctional Properties of Bulk Nanostructured Metallic Materials, Springer, Cham, 2015, pp. 27–100, https://doi.org/10.1007/978-3-319-19599-5_3.
[24] B. Jóni, E. Schafler, M. Zehetbauer, G. Tichy, T. Ungár, Correlation between the microstructure studied by X-ray line profile analysis and the strength of high-pressure-torsion processed Nb and Ta, Acta Mater. 61 (2013) 632–642, https://doi.org/10.1016/j.actamat.2012.10.008.
[25] J.M. Chae, K.O. Lee, A. Amanov, Gradient nanostructured tantalum by thermal-mechanical ultrasonic impact energy, Materials (Basel) 11 (2018), https://doi.org/10.3390/ma11030452.
[26] Y.S. Zhang, P.X. Zhang, H.Z. Niu, C. Chen, G. Wang, D.H. Xiao, X.H. Chen, Z.T. Yu, S.B. Yuan, X.F. Bai, Surface nanocrystallization of cu and Ta by sliding friction, Mater. Sci. Eng. A 607 (2014) 351–355, https://doi.org/10.1016/j.msea.2014.03.089.
[27] L. Kommel, P. Põdra, V. Mikli, B. Omranpour, Gradient microstructure in tantalum formed under the wear track during dry sliding friction, Wear. 466–467 (2021), 203573, https://doi.org/10.1016/j.wear.2020.203573.
[28] T.G. Langdon, Twenty-five years of ultrafine-grained materials: achieving exceptional properties through grain refinement, Acta Mater. 61 (2013) 7035–7059, https://doi.org/10.1016/j.actamat.2013.08.018.
[29] B. Omranpour, L. Kommel, V. Mikli, E. Garcia, J. Huot, Nanostructure development in refractory metals: ECAP processing of niobium and tantalum using indirect-extrusion technique, Int. J. Refract. Met. Hard Mater. 79 (2019) 1–9, https://doi.org/10.1016/j.ijrmhm.2018.10.018.
[30] L. Kommel, B.S. Omranpour, V. Mikli, Structuration of refractory metals tantalum and niobium using modified equal channel angular pressing technique, Key Eng. Mater. 799 (2019) 103–108, https://doi.org/10.4028/www.scientific.net/kem.799.103.
[31] L. Kommel, B. Omranpour Shahreza, Synthesis and characterization of mechanical properties of boron–carbon-based superhard composites, Carbon Lett. (2022), https://doi.org/10.1007/s42823-022-00351-9.
[32] A. Standard, G99, Standard Test Method for Wear Testing with a Pin-on-Disk Apparatus v, ASTM Int, West Conshohocken, PA, 2006, pp. 1–5.
[33] G. Ribárik, J. Gubicza, T. Ungár, Correlation between strength and microstructure of ball-milled Al-Mg alloys determined by X-ray diffraction, Mater. Sci. Eng. A 387–389 (2004) 343–347, https://doi.org/10.1016/j.msea.2004.01.089.
[34] F.H. Featherston, J.R. Neighbours, Elastic constants of tantalum, tungsten, and molybdenum, Phys. Rev. 130 (1963) 1324–1333, https://doi.org/10.1103/PhysRev.130.1324.
[35] A. Borbély, J. Dragomir-Cernatescu, G. Ribárik, T. Ungár, Computer program ANIZC for the calculation of diffraction contrast factors of dislocations in elastically anisotropic cubic, hexagonal and trigonal crystals, J. Appl. Crystallogr. 36 (2003) 160–162, https://doi.org/10.1107/S0021889802021581.
[36] B. Omranpour, L. Kommel, F. Sergejev, J. Ivanisenko, M. Antonov, M.A. L. Hernandez-Rodriguez, E. Garcia-Sanchez, Tailoring the microstructure and tribological properties in commercially pure aluminium processed by high pressure torsion extrusion, Proc. Est. Acad. Sci. 70 (2021) 540, https://doi.org/10.3176/proc.2021.4.23.
[37] E. Lorenzo-Bonet, M.A.L. Hernandez-Rodriguez, O. Perez-Acosta, M.A. De la Garza-Ramos, G. Contreras-Hernandez, A. Juarez-Hernandez, Characterization and tribological analysis of graphite/ultra high molecular weight polyethylene nanocomposite films, Wear. 426–427 (2019) 195–203, https://doi.org/10.1016/j.wear.2019.01.092.
[38] I. Hutchings, P. Shipway, Tribology: Friction and Wear of Engineering Materials, Second edition, Elsevier Inc, 2017.
[39] E. Hosseini, M. Kazeminezhad, Dislocation structure and strength evolution of heavily deformed tantalum, Int. J. Refract. Met. Hard Mater. 27 (2009) 605–610, https://doi.org/10.1016/j.ijrmhm.2008.09.006.
[40] G.C. Randall, K.R. Hansen, B. Jackson, D.T. Fullwood, Lower-bound dislocation density mapping in microcoined tantalum using high-resolution electron backscatter diffraction, Mater. Charact. 153 (2019) 318–327, https://doi.org/10.1016/J.MATCHAR.2019.04.033.
[41] P. La, J. Ma, Y.T. Zhu, J. Yang, W. Liu, Q. Xue, R.Z. Valiev, Dry-sliding tribological properties of ultrafine-grained Ti prepared by severe plastic deformation, Acta Mater. 53 (2005) 5167–5173, https://doi.org/10.1016/j.actamat.2005.07.031.
[42] G. Deng, X. Zhao, L. Su, P. Wei, L. Zhang, L. Zhan, Y. Chong, H. Zhu, N. Tsuji, Effect of high pressure torsion process on the microhardness, microstructure and tribological property of Ti6Al4V alloy, J. Mater. Sci. Technol. 94 (2021) 183–195, https://doi.org/10.1016/j.jmst.2021.03.044.
[43] C.T. Wang, N. Gao, M.G. Gee, R.J.K. Wood, T.G. Langdon, Effect of grain size on the micro-tribological behavior of pure titanium processed by high-pressure torsion, Wear. 280–281 (2012) 28–35, https://doi.org/10.1016/j.wear.2012.01.012.
[44] B. Omranpour, L. Kommel, F. Sergejev, J. Ivanisenko, M. Antonov, M.A. L. Hernandez-Rodriguez, E. Garcia-Sanchez, Analysis of the reciprocal wear testing of aluminum AA1050 processed by a novel mechanical nanostructuring technique, IOP Conf. Ser. Mater. Sci. Eng. 1140 (2021), 012051, https://doi.org/10.1088/1757-899x/1140/1/012051.
[45] B.O. Shahreza, M.A.L. Hernandez-Rodriguez, E. Garcia-Sanchez, L. Kommel, F. Sergejev, A. Salinas-Rodríguez, A. Heczel, J. Gubicza, The impact of microstructural refinement on the tribological behavior of niobium processed by Indirect Extrusion Angular Pressing, Tribol. Int. 167 (2021), 107412, https://doi.org/10.1016/j.triboint.2021.107412.
[46] G. List, G. Sutter, J.J. Arnoux, Analysis of the high speed sliding interaction between titanium alloy and tantalum, Wear. 301 (2013) 663–670, https://doi.org/10.1016/j.wear.2012.11.070.
[47] G. Sutter, J.J. Arnoux, G. List, P. Bourson, S. Margueron, H. Chaynes, Analysis of high friction conditions of Ti-6Al-4V alloy on tantalum by Raman spectroscopy and X-ray fluorescence, Tribol. Int. 57 (2013) 86–91, https://doi.org/10.1016/j.triboint.2012.07.008.
[48] C.T. Wang, N. Gao, R.J.K. Wood, T.G. Langdon, Wear behaviour of Al-1050 alloy processed by severe plastic deformation, in: Mater. Sci. Forum, Trans Tech Publications Ltd, 2011, pp. 1101–1106, https://doi.org/10.4028/www.scientific.net/MSF.667-669.1101.